Atmospheric Environment 125 (2016) 199–211

Contents lists available at ScienceDirect

Atmospheric Environment

journal homepage: www.elsevier.com/locate/atmosenv

Secondary effects of urban heat island mitigation measures on air quality

Joachim Fallmann*, Renate Forkel, Stefan Emeis

Institute of Meteorology and Climate Research, Atmospheric Environmental Research (IMK-IFU), Karlsruhe Institute of Technology, Garmisch-Partenkirchen, Germany

HIGHLIGHTS

- We model impacts of urban heat island mitigation measures on air quality.
- Liaison of a multi-layer urban canopy model and WRF-Chem.
- Urban greening and white roofs decrease average ozone concentration.
- We find an increase of primary pollutants due to reduced vertical mixing.
- Peak ozone concentration increases for white roofs due to short-wave reflection.

GRAPHICAL ABSTRACT

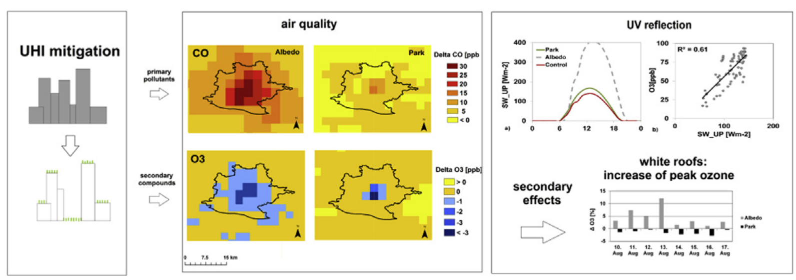

ARTICLE INFO

Article history:
Received 24 April 2015
Received in revised form 29 October 2015
Accepted 31 October 2015
Available online 14 November 2015

Keywords:
Urban heat island mitigation
Air quality
WRF-Chem
Urban canopy model
Turbulence
Ozone photochemistry

ABSTRACT

This study presents numerical simulations analysing the effect of urban heat island (UHI) mitigation measures on the chemical composition of the urban atmosphere. The mesoscale chemical transport model WRF-Chem is used to investigate the impact of urban greening and highly reflective surfaces on the concentrations of primary (CO, NO) as well as secondary pollutants (O_3) inside the urban canopy. In order to account for the sub-grid scale heterogeneity of urban areas, a multi-layer urban canopy model is coupled to WRF-Chem. Using this canopy model at its full extend requires the introduction of several urban land use classes in WRF-Chem. The urban area of Stuttgart serves as a test bed for the modelling of a case scenario of the 2003 European Heat Wave. The selected mitigation measures are able to reduce the urban temperature by about 1 K and the mean ozone concentration by 5–8%. Model results however document also negative secondary effects on urban air quality, which are closely related to a decrease of vertical mixing in the urban boundary layer. An increase of primary pollutants NO and CO by 5–25% can be observed. In addition, highly reflective surfaces can increase peak ozone concentration by up to 12% due to a high intensity of reflected shortwave radiation accelerating photochemical reactions.

1. Introduction

The excessive warming of impervious surfaces and additional release of anthropogenic heat promotes urban heat island (UHI) formation. Human activities lead to an increase of emissions of air pollutants which in turn influences the chemical composition of

* Corresponding author.
E-mail address: joachim.fallmann@kit.edu (J. Fallmann).

http://dx.doi.org/10.1016/j.atmosenv.2015.10.094
1352-2310/

urban air.

The annual mean temperature of the central areas of a large city is about 1–3 °C higher than in the surrounding areas. In calm clear nights, city centres can be as much as 12 °C higher (Oke, 1982). Additional heat generated by fuel combustion, air conditioning or human activities, as well as the slowing down of wind speed due to roughness effects caused by building structures, help to 'design' specific atmospheric dynamics. The resulting secondary urban-rural circulation patterns can, in turn, promote dispersion of pollutants into rural surroundings (Arnfield, 2003). Detailed documentations of the urban heat island effect exist for several major cities in the world (Santamouris, 2007).

The number of publications concerning UHI research has been continuously increasing recently, with regard to both modelling (Giannaros et al., 2013; De Ridder et al., 2015) and remote sensing observations (Zaksek and Ostir, 2012; Tam et al., 2015). Diurnal variations of the surface UHI under ideal weather conditions were discussed for Bejing (Zhou et al., 2013), showing significant UHI effects from late morning to night. Analysing measurement data for the urban area of London, Barlow et al. (2015) described the different boundary layer characteristics over urban and rural surfaces which control urban flow and dispersion.

Specific measures like green roofs or facades and highly reflective materials are able to reduce the UHI. Taha (1997b) demonstrated that increasing the albedo by 0.3 can reduce peak summertime temperatures for the urban area of Los Angeles by up to 1.5 °C. During the DESIREX Campaign 2008, Salamanca and Martilli (2012) stated that a higher albedo leads to a 5% reduction in energy consumption by air conditioning during summertime periods for the area of Madrid. The regional energy saving effect of high-albedo roofs can also be found in Akbari et al. (1997) and on a more global perspective in Akbari et al. (2009). Georgescu et al. (2014) analysed the potential of green roofs and highly reflective roofs to reduce the urban induced warming of the United States by 2100. They could prove, that the decrease of average summer near surface temperature achieved by area wide hybrid measures (mixture between white and green roofs) could compensate the projected temperature increase for the period 2079–2099 compared with 1990–2010 for California, Texas, Mid-Atlantic and the area Chicago/Detroit. Schubert and Grossman-Clarke, 2013 stated the positive effect of urban greening and increased surface albedo on temperature for heat wave conditions in the city of Berlin.

The relation between urban heat island and air quality was investigated in Lai and Cheng (2009) who combined observation data and air quality simulations for the urban area of Taichung. They found that a stable high pressure system followed after the departure of a typhoon favoured both, UHI formation and an increase of ozone, $PM_{2.5}$ and PM_{10} concentrations due to stagnant weather conditions within the basin. Akbari et al. (2001) stated that urban trees and high-reflective roofs can significantly reduce energy consumption, thus improving air quality. Recent studies (Sarrat et al., 2006) showed that the availability and spatial distribution of urban pollutants is significantly modified by the urbanized area due to enhanced turbulence. A recent WRF-Chem modelling study analysed the impacts of mixing processes in the nocturnal atmospheric boundary layer on urban ozone concentrations (Klein et al., 2014). Modelling and measurements showed that near-surface ozone concentrations were higher during less stable nights when active mixing persisted, due to increased dispersion of nitrogen oxide responsible for ozone titration as well as downward mixing of ozone from the residual layer to the surface. The impact of atmospheric stability upon near-surface concentration of pollutants is stated by Wood et al. (2013) who used ground based remote sensing techniques in the urban area of Helsinki. Highest particle concentrations were measured during stable conditions or in the stability transition from stable to neutral.

Taha (1997a; 2008) found a decrease in peak ozone concentrations between 1400 and 1600 h local time in the urban areas and downwind of Los Angeles and Sacramento when the surface albedo in the urban areas was increased from 0.2 to 0.5. As discussed later in this paper in more detail we found an increase of peak ozone levels when increasing the albedo of building roofs and facades from 0.2 to 0.7.

In the current study, we use WRF-Chem (Grell et al., 2005) with an urbanized version of WRF (Chen et al., 2011; Martilli et al., 2002; Kusaka et al., 2001) to investigate the effect of urban heat island mitigation measures on air quality. The multi-layer urban canopy model BEP (Martilli et al., 2002) is coupled to the chemical transport model WRF-Chem. Technical modifications of the input data and certain modelling schemes were carried out, allowing for a more diverse representation of the urban land use within the model.

The urban area of Stuttgart located in south-west Germany acts as test bed for different scenario simulations. The main objective of this study is to investigate the effect of different UHI mitigation measures on urban air quality. In general it aims to ponder the role of dynamical and chemical processes in the urban boundary layer on the concentration of primary and secondary pollutants within the urban canopy. Three different scenario simulations are carried out, considering urban greening, highly reflective roofs and facades as well as a changed building density.

Whereas existing studies mainly concentrate on the effects on urban ozone concentrations, our study describes the full gas phase urban chemistry including primary pollutants as well. The urban heat island mitigation scenarios which are tested for their effect on urban air quality have been presented by Fallmann et al. (2014). This study found a decrease of the daily averaged urban heat island intensity for Stuttgart for both urban greening and increased surface reflectivity by 1.1 and 1.7 °C respectively.

The first part of this paper documents the methodology of modifying WRF-Chem and processing the input data. Further the process of setting up the urban canopy model for the urban area of Stuttgart with regard to the selected scenarios is presented. Chapter 3 shows the model evaluation for a base case model run. The modelling results and discussion parts follow in Chapter 4 and 5. The latter Chapter separates primary and secondary pollutants and takes tendency terms into account pondering dynamical and chemical effects. A concluding Chapter summarizes the results and provides an outlook on future studies.

2. Data and methods

2.1. Model setup

The chemical transport model WRF-Chem Version 3.5.1 (Grell et al., 2005) is used. The model domain is setup for an area of 200 by 150 grid cells with a horizontal resolution of 3 km (Fig. 1). This grid size still allows for a considerable number of urban grid cells for the area of Stuttgart. The domain does neither extend into areas of higher surface elevation in the south, nor into the North Sea, which both could lead to errors at the domain borders. The vertical dimension is resolved by 36 levels, with 6 levels located in the lowest 100 m. The modelling period ranges from Aug 09 to Aug 18 2003, a heat wave period which can be seen as a proxy for future climate conditions in Europe (Vautard et al., 2007). The first day is seen as spin up and therefore removed from further analysis.

The Building Effect Parameterization BEP (Martilli et al., 2002) scheme is coupled to WRF-Chem and used as described in Chen et al. (2011). The multi-layer BEP accounts for the three-

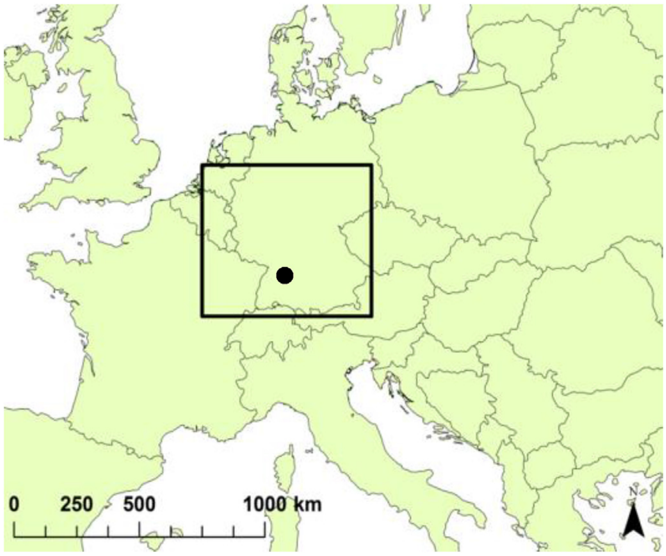

Fig. 1. WRF-Chem model domain (black frame) and the location of the city of Stuttgart (black dot).

dimensional nature of urban surfaces and treats the buildings as sources and sinks of heat, moisture and momentum. The effects of horizontal (roofs, roads) and vertical (walls) surfaces on the turbulent kinetic energy (TKE), potential temperature (Θ) and momentum are also covered by this model. The BEP treats several layers within the urban canopy, allowing a high vertical resolution close to the ground and a direct interaction with the urban boundary layer.

The building energy model BEM (Salamanca and Martilli, 2012) is not used, because test runs showed an influence on meteorological and chemical variables of less than 5%. In the course of the study, the urbanized WRF-Chem model is referred to as 'WRF_BEP'.

The MACC 7 km emission inventory for the year 2003–2007 (Kuenen et al., 2011) is used for anthropogenic emissions. Biogenic emissions originate from the global MEGAN emission database (Guenther et al., 2012). Lateral chemical boundary conditions are obtained from MOZART output (Emmons et al., 2010). The RADM2 (Regional Acid Deposition Model) scheme is applied for calculating the gas-phase chemistry, aerosol dynamics and chemistry is described with the module MADE/SORGAM (Ackermann et al., 1998; Schell et al., 2001).

WRF-Chem offers various gas phase chemistry options. The RADM2/MADE/SORGAM option was chosen for this study since it is widely used for regional air quality simulations due to its wide coverage of chemical regimes and its comparatively low numerical costs. According to Knote et al. (2015) the uncertainty in predicted ozone during summer due to the choice of the chemical mechanism is 5%. With regard to ozone, the performance of the RADM2 mechanism in regional models is similar to more recent and complex mechanisms (e.g. Im et al., 2015).

For both longwave- and shortwave radiation the RRTMG scheme (Mlawer et al., 1997) is applied. The microphysics is based on the Lin et al. (1983) scheme. Turbulent fluxes of heat, momentum and constituents within the atmospheric boundary layer are parametrized within the Mellor–Yamada–Janjic (MYJ) planetary boundary layer scheme (Hu et al., 2010). The Grell-Devenyi Ensemble Scheme (Grell and Devenyi, 2002) is used for cumulus parametrization and the land surface processes are described with the Noah-LSM, a multi-layer soil model that includes prognostic equations for the soil temperature and soil liquid water content (Mitchell, 2005). Similar to the meteorological initial and boundary conditions the initial soil temperature and moisture is derived from 0.5 deg. ERA-Interim fields (Dee et al., 2011). The full setup used for WRF_BEP is summarized in Table 1.

2.2. Input data and pre-processing

Urban areas are classified by grid cells with the land use index 31 (low density residential), 32 (high density residential) and 33 (industrial and commercial). The three urban classes are distinguished based on their appearance and percentage of impervious surface. Low intensity residential (class 31) includes areas with a mixture of constructed materials and vegetation, with vegetation accounting for 20–70% of the land cover. Similarly, vegetation is under 20% for high-density residential areas (class 32). Industrial/commercial (class 33) includes infrastructure and highly developed areas not classified as residential (USGS, 2006).

In the current version of WRF-Chem, a 24 class land use classification is implemented by default, which does not allow for a differentiation of urban land in the model (Fig. 2a).

In order to represent the heterogeneity of urban land surfaces and to use the urban canopy model at its full extend the original urban class (1) is divided into 3 subclasses (31–33) in WRF-Chem (Fig. 2b). The class numbers 31–33 have been chosen in accordance to the BEP. The land use classes 25–30 are not used in the new dataset.

As dry deposition is controlled mainly by the land use type, the land use categories for urban areas have to be initialized within the source code of the dry deposition module as well. In order to compute the total surface resistance to gaseous dry deposition r_c and the deposition velocity respectively, input parameters must be defined for all 33 classes being classified in the land use input data. Dry deposition is responsible for a large portion of removal of trace chemicals from the atmosphere whereas the rate can be calculated from the total surface resistance (Wesely, 1989, Wesely and Hicks, 2000). Analogue to Ohm's law in electric circuits, surface resistance is calculated for 11 Wesely types. Due to a lack of reference data, the land use classes 31: 'low density residential', 32: 'high density residential' and 33: 'industrial/commercial' are combined to Wesely class 1 ('Urban Land'). The seasonal class is set to 1: 'midsummer with lush vegetation'. All the terms describing the surface resistance are retrieved from Wesely (1989). Analogue to dry deposition, the correct number of land use classes has to be initialized in the biogenic emission module as well. In general, a biogenic emission factor of zero is assigned for urban land use.

In order to account for the morphological features of the urban area of Stuttgart, the characteristics of roads and buildings have to be defined within the BEP. The mean road widths and -orientations are estimated from grid cell equivalent google earth extracts (approximately 3 × 3 km) representing 3 different urban classes related to the land use types in Fig. 2b. All roads within these boxes are measured and the average road width is calculated. The mean size of building roofs is calculated in the same way. The mean building height for each urban class is retrieved from a high resolution digital elevation model resolving each building in the urban area of Stuttgart. This data has been supplied by the Land Surveying Department Stuttgart. Urban morphological parameters considered within BEP are presented in Table 2.

The thermal conductivity, specific heat capacity, emissivity, albedo and roughness length of momentum is defined for roofs, walls and road. The values are taken from Salamanca and Martilli (2012).

2.3. Scenarios

A base case (Control) and three scenario runs are conducted, applying the BEP scheme (Martilli et al., 2002). The WRF-Chem

Table 1
WRF_BEP model configuration.

Parameter/scheme	Specification	Parameter/scheme	Specification	Parameter/scheme	Specification
Geographical input data	1 km USGS land use	Meteorological BC	0.5 Deg ERA-Interim	Land surface model	Noah LSM
dx, dy	3 km	Urbanization scheme	BEP (Martilli et al., 2002)	Chemical option	RADM2, MADE/SORGAM aerosols
West-east [grid cells]	200	Microphysics	Lin et al.		
South-north [grid cells]	150	Longwave	RRTMG (Mlawer et al., 1997)	Emission inventory	7 km MACC 2006
Vertical layers	36	Shortwave	RRTMG	Chemical boundary	MOZART global data
Time frame	8/9–8/18/03	Cumulus (only 3rd domain)	Grell Devenyi ensemble	Biochemistry	MEGAN global data
Lowest model level	8.5 m	Land surface model	Noah LSM	Photolysis scheme	FastJ

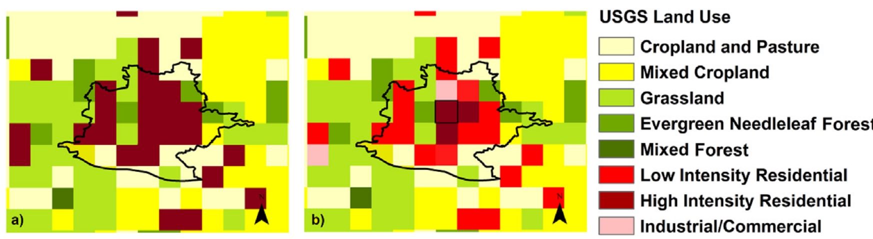

Fig. 2. Extract of the WRF land use input data for the original 24 class land use (a) and the new 33 class land use (b). The black line indicates the boundary of the city of Stuttgart. The black square in the centre indicates the location of the grid cell used for model evaluation (b).

Table 2
Street and building parameters and distributions of building heights as defined in the multi-layer urban canopy model BEP.

Height [m]	Class 33	Class 32	Class 31
Urban fraction	0.9	0.8	0.6
% of buildings with 5 m height	44	33	48
% of buildings with 10 m height	26	20	37
% of buildings with 15 m height	14	23	11
% of buildings with 20 m height	8	18	3
% of buildings with 25 m height	4	4	1
% of buildings with 30 m height	2	2	–
% of buildings with 35 m height	2	–	–
Street width [m]	19	15	18
Building width [m]	25	13	10

scenarios represent well-established urban planning strategies like urban greening (Park), increased surface albedo (Albedo) or changed building density (Density). For the urban greening scenario, two urban grid cells in the centre of Stuttgart, accounting for 9% of the total urban area, are replaced with grassland (Fig. 3).

The land surface model NOAH-LSM in WRF calculates the heat and water balance for vegetation covered surfaces and the heat balance for dry sealed surfaces. A change of a grid cell from urban type to grassland (Fig. 3b) infers a change of the fraction of the vegetation covered surface from 0.12 to 0.8 and a change of the fraction of the non-evaporating surface from 0.88 to 0.2. At the same time as the vegetation fraction is changed from 0.12 to 0.8 the roughness height z_0 is decreased from 1.2 m to 0.12 m for the respective grid cells. The values are obtained from the default settings of WRF Version 3.5 (Wang et al., 2011).

An increased albedo of roofs and facades is simulated by changing the surface albedo for all grid cells with urban land use from 0.2 to 0.7 which represents a highly reflective white paint (Takebayashi and Moriyama, 2007). This modification enhances the reflected solar radiation of the built-up area and by this modifies the total heat flux from the surface to the lowest atmospheric layer.

The change of the building density is the third scenario which is analysed. In our simulations we increase the main road width in the BEP urban canopy table from 19 to 22 m (class 33), from 15 to 18 m (class 32) and from 18 to 21 m (class 31). The rest of the urban properties remain consistent to the base case. This modification implies an increase of the roof/road ratio within the urban canopy table by 20%. This has an effect on the distribution of heat within the urban canyon considering shadowing, reflections and trapping of shortwave and longwave radiation (Chen et al., 2011).

3. Model evaluation

The WRF_BEP simulations are evaluated for the Control run at an urban grid cell located in the centre of Stuttgart (Fig. 2b). Simulated concentrations of primary and secondary compounds within the lowest model level are compared with the average of three existing urban measurement stations (Table 3) located within that specific model grid cell (Table 4).

Each station is located at a similar geographical height asl. Two stations are located at street level (urban/road), in close proximity to local emission sources. The third station is installed at roof level (urban/roof) in the urban centre. Averaging over the three measurement heights gives a mean height of 10.3 m which represents

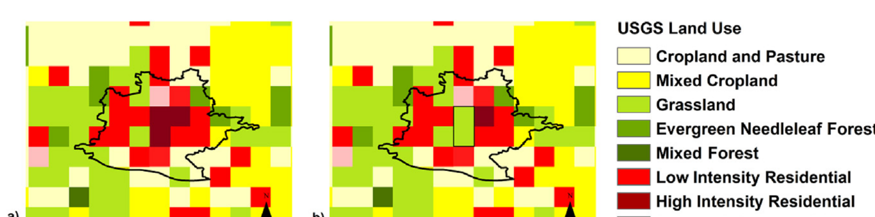

Fig. 3. Land use change comparing the base case (a) and the urban greening scenario (b) for the urban area of Stuttgart (black line) and the surrounding grid cells. The black rectangle indicates the grid cells where urban land use is replaced by a park.

Table 3
Characteristics of three air quality measurement sites located within the respective urban grid cell (Fig. 2b) used for the comparison between model and measurement.

Nr	Station	Type	Altitude a.s.l. [m]	Measurement height [m]	Model orography [m]	Model analysis height [m]	Provider
1	Mitte – Arnulf Klett-Platz	urban/road	245	25	253	8.5	LUBW
2	Schwabenzentrum	urban/roof	250	3.5	253	8.5	Envir. Prot. Agency Stuttgart
3	Bad Cannstadt – Gnesener Str.	urban/road	235	2.5	253	8.5	LUBW

Table 4
Comparing observations (mean value for 3 stations) with the base case (WRF_BEP) for the modelling time period Aug 10 – Aug 18 2003. Calculation of absolute (Bias_abs) and relative bias (Bias_rel), correlation coefficient R and absolute biases for night and day. Results are shown for secondary (ozone) and primary pollutants (NO, NO_2, CO) as well as meteorological parameters potential temperature (TH_2), wind speed (U10), relative humidity (RH) and incoming shortwave radiation (SR).

	OBS	WRF_BEP	Bias_abs	Bias_rel	R [-]	Bias_night	Bias_day
O_3 [ppb]	41.9	40.1	−1.8	−0.04	0.73	−7.6	2.0
NO [ppb]	9.3	4.7	−4.6	−0.49	0.56	−5.6	−3.9
NO_2 [ppb]	31.3	20.9	−10.3	−0.33	0.61	−1.7	−16.4
CO [ppb]	375.2	352.3	−22.9	−0.06	0.16	−29.0	−68.0
TH_2 [°C]	24.8	25.6	0.8	–	0.88	1.5	0.9
U10 [ms^{-1}]	1.0	1.1	0.1	–	0.54	0.1	0.1
RH [%]	43.2	45.4	2.2	–	0.3	1.7	2.1
SR [Wm^{-2}]	501.0	451.0	−50.0	–	0.97	–	–

the grid cell average for the first model level (~8.5 m).

Mean diurnal variations for ozone, CO, NO_2 and NO are computed for the base case simulation (WRF_BEP) and compared with observations (OBS) (Fig. 4).

All times in the following discussion refer to the Central European SummerTime (Daylight Saving Time) (CEST).

Peak ozone concentrations within the modelling period range from 80 to 100 ppb. The model shows a slight underestimation of ozone during the night and a minor overestimation during the day (Fig. 4a). The too low ozone concentrations during the night might be due to an underestimation of the ozone concentrations found in the residual layer or a too weak downward mixing of ozone from the residual layer towards the surface. Since ozone in the nocturnal residual layer is not depleted by titration and dry deposition, concentrations during the night are higher there than near the surface. The importance of vertical mixing for nocturnal near surface ozone concentrations has been reported by several studies (Zhang and Rao 1999; Klein et al., 2014). The general uncertainty of simulated ozone concentrations in the mid-latitudes by several mesoscale air quality models is discussed by Im et al. (2015). Besides the quality of the chemistry mechanism, the parameterization of dry deposition and the general quality of the meteorological forecast, uncertainties in the emissions inventories of precursor substances can be considered to be a reason for errors in simulated ozone concentrations.

For long lived chemical species like CO (Fig. 4b), the too low concentrations for well mixed conditions during the daytime can partly be attributed to too low boundary values. The MACC dataset which is used in this study, in general shows negative biases for the European domain (Giordano et al., 2015). The peak of CO at around 8 am is captured quite well, with WRF_BEP overestimating the observation by 61 ppb (10%).

For the shorter lived species such as NO_x the effect of boundary conditions is minor (Giordano et al., 2015).

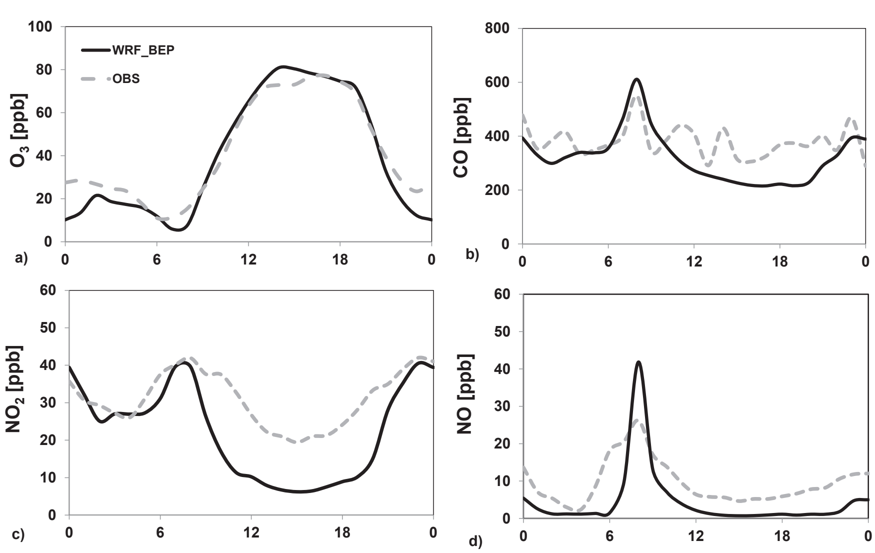

Fig. 4. Diurnal variations of modelled concentration of Ozone (a), CO (b), NO_2(c), NO (d) at an urban grid cell using BEP (black) in comparison with the mean of observations from 3 measurement stations located within that grid cell (grey dotted). The curves represent average values for the episode August 10–18 2003.

With regard to NO_2, the morning concentrations are reproduced quite well, but WRF_BEP tends to underestimate the daytime values by over 60% (Fig. 4c). Overestimation of daytime vertical mixing may be one reason for the underestimation of near surface NO_2. If more NO is removed by daytime turbulence near the surface, less is available for the production of NO_2 near the surface (Seinfeld and Pandis, 2012).

NO concentration is found to be too low for the whole period, except for the morning rush hour peak, where WRF-Chem overestimates the observation by 16 ppb (~60%). Although the diurnal profile of the emissions seems to be reproduced quite well, the overestimation during the rush hour peak might be caused by the fact that the diurnal evolution of the boundary layer is slightly delayed, which immediately leads to an underestimated mixing.

The relative biases for simulated primary and secondary compounds range from −0.04 for ozone to −0.49 for NO, the daytime biases exceeding nighttime biases for NO_2 and CO and the other way round for NO. Daytime bias of ozone is negative during the day, whereas it is positive during the night. Correlations between WRF_BEP and OBS are above 0.5, except for CO.

In general, temperature is overestimated by 0.8 °C with improved performance found during the day. The low observed wind speed for the investigated summer period can be reproduced by WRF_BEP. The correlation coefficient is over 0.5 for temperature, wind speed and radiation but is only 0.3 with regard to relative humidity. Although the grid cell resolution of 3 km seems to be too coarse for simulating flow pattern in complex terrain, intensive testing showed that WRF_BEP is able to reproduce general wind speed and wind directions within the area. The biases of the absolute values do not disturb the main aim of this study since we are mainly interested in the relative changes between the scenario cases and the base case.

4. Results of scenario simulations

4.1. Effect on meteorology

Mean values of potential 2 m temperature (TH_2), 10 m wind speed (U10), turbulent kinetic energy (TKE) and planetary boundary layer height (PBLH) as well as downward and upward shortwave radiation (SW) are presented in Table 5 to document the effect of the scenarios on meteorological conditions. TKE and PBLH are included in this table, as turbulent exchange affects the distribution and vertical dilution of primary emitted pollutants within the urban canopy. The TKE term is prognostically calculated and used to determine eddy diffusion coefficients within the MYJ boundary layer scheme (Janjic, 1990, 2001). The PBLH is defined by the height, at which 2*TKE first drops below 0.2 $m^{-2}s^{-2}$ (Mellor and Yamada, 1982). Averaging period is Aug 10 – Aug 18 2003. Daytime means (0700–2000 CEST) are indicated in bold, nighttime means (2100–0600 CEST) in italics.

In average, the temperature is reduced by 1.2 °C and 1.3 °C for the Albedo and Park scenario, respectively. An increased surface reflectivity (Albedo) results in a stronger temperature decrease during the day than for the period between 2100 and 0600 CEST. For urban greening (Park) however, the cooling effect during the night outperforms the Albedo scenario. For the Density scenario, only a minor effect on temperature is observed, for both day- and nighttime.

The mean wind speed is low during the model period and the relative decrease from base case to Albedo is almost 50%. The high relative decrease of wind speed might be due to the fact that the lower near surface temperature in the city for the Albedo case leads to a loss of the buoyancy production term in the TKE production equation which results in a decrease of friction velocity u* (Stull, 1988). For the urban greening scenario a small increase in U10 is observed in the urban centre due to a decrease in roughness height by the removal of buildings. This effect seems to outperform the temperature effect. Density shows no effect on wind speed.

On a daily average, reductions of the TKE by about −0.1 m^{-2} s^{-2} and the PBLH by about −50 m and −80 m can be observed for the Albedo and the Park scenario, respectively. The reduction in turbulent mixing and boundary layer height is predominantly attributed to the daytime (bold) with a simulated decrease of the TKE by of −0.16 $m^{-2}s^{-2}$ and a PBLH reduction of −84 m with respect to Albedo. During nighttime (italics), the effect can be neglected for this scenario. The decrease of the PBLH with regard to the urban greening scenario (Park) accounts for −124 m during the day and −22 m during the night. The bigger nighttime boundary layer effect can be attributed to evaporative cooling of vegetation surfaces at night. When decreasing the building density (Density), WRF-Chem does not show an impact on TKE and PBLH. Increasing the albedo of building materials leads to an increase of the reflected shortwave radiation. For Control and Density, about 17% of the daytime mean incoming shortwave radiation at the surface is reflected, whereas this value accounts for about 20% for Park and up to 50% for Albedo. The difference in reflected shortwave radiation (SW_UP) between Park and Control can be attributed to the change of the albedo for built up areas (0.15) to the value for grassland (0.20). The almost non-existent difference of the solar radiation between the base case and Density can also explain the very small effect of this scenario on temperature. It seems that changing the building density by a small percentage only has a small sensitivity on temperature, wind speed and mixing within the BEP urban canopy model.

4.2. Effect on pollutant concentrations

Table 6 shows mean near surface (at 8.5 m) concentrations of NO, NO_2, CO and ozone on the basis of mean values for an area of 2 × 2 grid cells in the urban centre for the base case (Control) and the three scenarios.

In general, a decrease of near surface air temperature results in an increase of primary pollutants such as NO and CO. NO_2 partly

Table 5
Effect of UHI mitigation scenarios on 2 m potential temperature (TH_2), 10 m wind speed (U10), turbulent kinetic energy (TKE), planetary boundary layer height (PBLH), and downward and upward shortwave radiation at the surface (SW) in the urban centre (2 × 2 grid cells). Values are presented for the mean of the modelling period Aug 10–18 2003. Daytime mean values are shown in bold, night-time values in italics.

Scenario	Control	Albedo	Park	Density
TH2 [°C]	26.8 (**29.6**, *21.9*)	25.6 (**28.3**, *21.6*)	25.5 (**28.6**,*20.4*)	26.6 (**29.3**, *21.7*)
U10 [ms-1]	1.1 (**1.1**, *0.65*)	0.65 (**0.9**, *0.7*)	1.3 (**1.4**, *1.0*)	1.0 (**1.1**, *0.65*)
TKE [$m^{-2}s^{-2}$]	0.34 (**0.46**, *0.11*)	0.23 (**0.30**, *0.11*)	0.22 (**0.28**, *0.11*)	0.33 (**0.45**, *0.11*)
PBLH [m]	563 (**874**, *64*)	519 (**790**, *62*)	485 (**750**, *42*)	567 (**871**, *68*)
SW_Down [Wm^{-2}]	**499**	**503**	**500**	**497**
SW_Up [Wm^{-2}]	**86**	**250**	**106**	**85**

Table 6
Effect of UHI mitigation measures on modelled episode mean, daytime mean (bold) and nighttime mean (italics) concentrations of NO, NO_2, CO and ozone in the urban centre (mean of 2 × 2 urban grid cells) for the lowest model level (8.5 m). Values are presented for the mean of the modelling period Aug 10–18 2003 in ppb.

Scenario	Control	Albedo	Park	Density
NO [ppb]	4.7 (**6.1**, *2.3*)	5.8 (**7.8**, *2.6*)	4.9 (**6.4**, *2.5*)	4.8 (**6.2**, *2.4*)
NO_2 [ppb]	20.6 (**14.5**, *30.8*)	23.4 (**17.3**, *33.7*)	22.0 (**16.1**, *31.7*)	20.7 (**14.5**, *31.7*)
CO [ppb]	366.7 (**292**, *432.3*)	398.8 (**362.6**, *457.6*)	381.9 (**345.8**, *440.4*)	373.1 (**307.8**, *435.4*)
O_3 [ppb]	40.1 (**54.9**, *15.3*)	38.4 (**52.8**, *14.3*)	36.9 (**50.4**, *14.5*)	39.9 (**54.6**, *15.2*)

originates from primary emission but also from NO titration. With regard to NO and CO, the strongest effect is found for the Albedo case. The increase of mean NO concentration amounts to over 25%, mean CO concentration is increased by about 9% for this scenario. Urban greening (Park) tends to increase both compounds by 5% and 4% respectively. Nitrogen dioxide is increased by 14% and by 7% with regard to Albedo and Park respectively. Reducing the air temperature however is able to decrease mean ozone concentration by 6% (Albedo) and 8% (Park). The small effect of changed building density on meteorology (Table 5) results in a minor effect on pollutant concentration. Therefore, Density is omitted in the following discussions.

The spatial effects of the scenarios on the urban area of Stuttgart are presented in Fig. 5 for CO (a) and ozone (b). Fig. 5 shows an extract of the WRF-Chem model domain of 13 × 13 grid cells with the area of Stuttgart located in the centre. A horizontal resolution of 3 km infers that the greater Stuttgart urban area is represented by about 22 grid cells. Dark colours indicate a large impact on near surface concentration – which is positive for primary- and negative for secondary pollutants. Bright colours imply minor or zero effects.

While the effect on primary pollutants is most pronounced for the albedo scenario (5a), with a maximum mean concentration increase of 32 ppb (8.7%) the situation is reversed for ozone (Fig. 5b) with a maximum mean decrease of 3.2 ppb (9.2%) for the Park scenario.

In addition to Table 6 and Fig. 5, mean relative concentration differences between scenario and base case (Control) are shown in Fig. 6, separating between nighttime and daytime.

Although the absolute concentrations of NO_2 and CO are higher during the night than during the day, the relative impact of reduced temperature is more pronounced during the day except for NO for Park. Strongly depending on local emission sources, daytime NO_x and CO concentrations are higher for the scenarios than for the base case simulation, since both scenarios result in a reduced warming near the ground and therefore in reduced turbulent exchange. This effect is more pronounced for Albedo than for the urban greening scenario Park. With regard to the urban greening scenario, relative daytime effects are stronger except for NO. The latter however generally shows very low concentrations at night (Table 6), leading to small changes resulting in large relative effects. In our study, increasing the albedo of the built-up area results in a more pronounced decrease of the mean ozone concentration during the night than during the daytime, since during the day, additional ozone can be formed due to increased photolysis rates over the highly reflecting surfaces.

4.3. Diurnal variation

Fig. 7 shows relative hourly mean (mean over the same hour of the day for all days of the episode) differences between the scenarios (Albedo, Park) and the base case for the near surface concentration of ozone, NO_x and CO.

In general, the diurnal courses document the same findings as indicated in Chapter 4.2, with a decrease of secondary and an

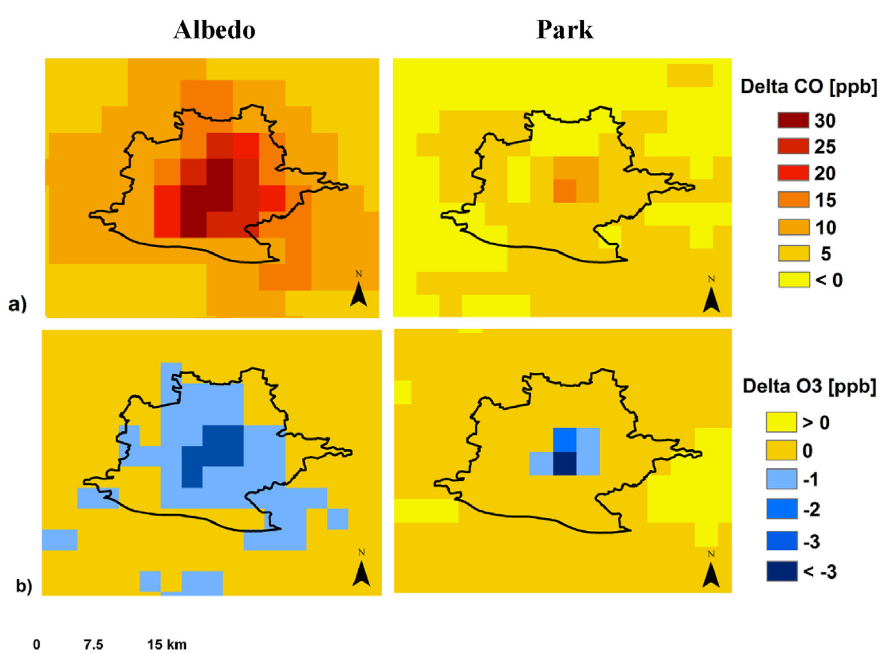

Fig. 5. Absolute difference between scenario run and base case for simulated mean CO (a) and ozone (b) concentrations [ppb] in the lowest model level. The Albedo scenario is shown on the left and the Park scenario on the right.

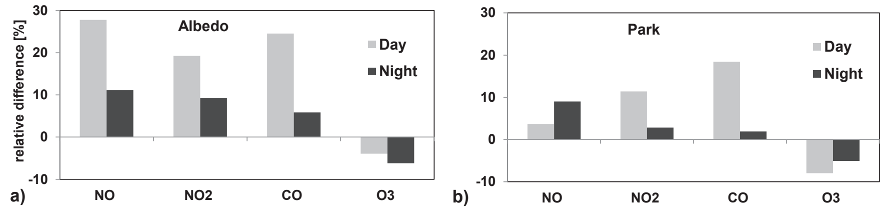

Fig. 6. Relative difference between mean value of both scenario runs and the base case (Control). Daytime values are shown in grey, nighttime values in black. Values are calculated for NO, NO_2, CO and O_3 with negative values indicating a relative decrease, positive values and increase in mean near surface concentration.

increase of primary compounds. The strong decrease of the ozone concentration for the urban greening scenario during the evening hours (Fig. 7a) can be explained by stronger surface cooling over vegetative surfaces than over the impervious surfaces. Turbulent mixing is decreased in particular during the forenoon for both scenarios, which reduces the downward mixing of ozone from higher levels during this time (Velasco et al., 2008; Klein et al., 2014). Additionally, a larger amount of ozone is removed via NO_x titration. In general, the highest relative decrease of ozone is congruent with the highest levels of NO_x (Fig. 7b).

The high relative increase of daytime NO_x can be attributed to NO, which is emitted and hampered from being diluted due to weaker atmospheric turbulence. In the course of a day NO is interconverted to NO_2, which gradually builds up during the day. NO which is emitted in the evening quickly reacts with ozone to form NO_2 again, leading to higher relative increases in NO_2 there (Fig. 7b). With regard to CO the morning peaks are higher for Albedo due to the considerable slowdown of surface temperature increase of the highly reflective surfaces in the morning hours (Fig. 7c), which results in a reduced vertical turbulent exchange during this time.

For the Albedo case a small positive peak in relative mean hourly ozone change can be observed between 1400 and 1600 CEST (Fig. 7a). This effect can be explained by the higher reflected shortwave radiation (Table 5), leading to an increase in the episode mean hourly maximum ozone concentration by up to 4.5%. Fig. 8 shows the relative increase of daily peaks of the ozone concentration between 14 and 16 CEST for the single days of the episode. Differences can reach up to 10 ppb (12%) for the Albedo scenario. For the urban greening scenario (Park) a small decrease of the peak ozone concentrations is found for all days. Possible reasons for this difference between the Albedo and the Park scenario will be discussed in Section 5.3 of this paper.

5. Discussion

5.1. Primary compounds

The concentration of primary compounds as simulated for the lowest model layer is negatively correlated to the dynamic variable

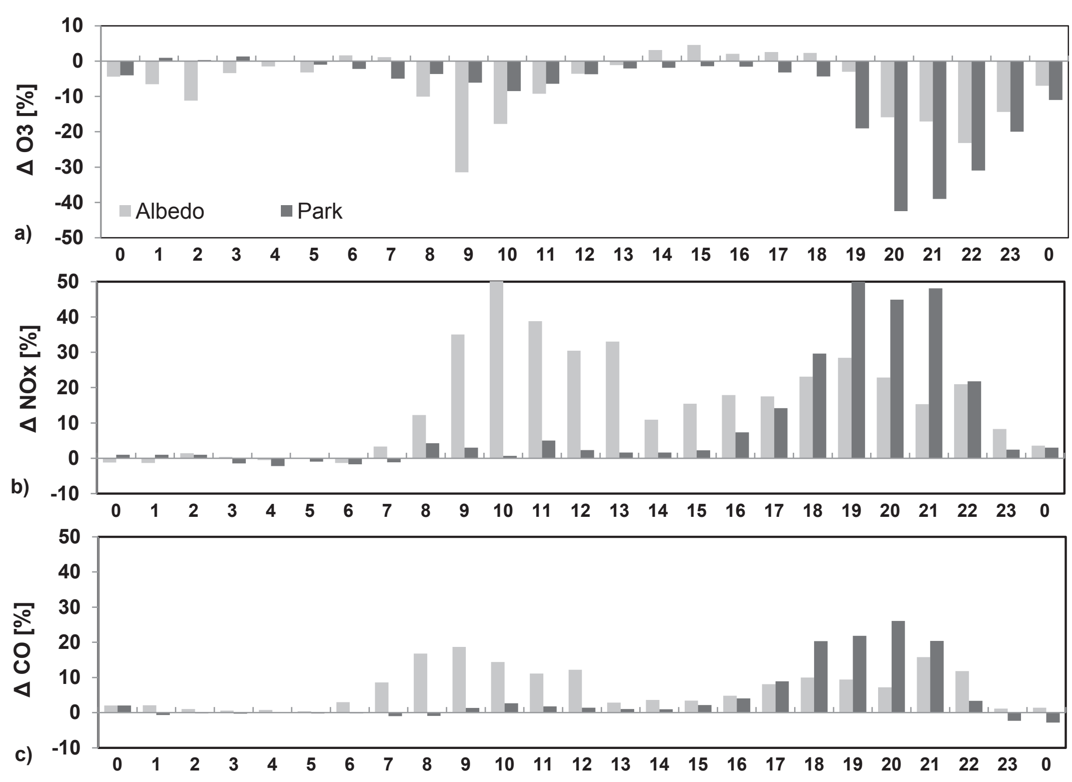

Fig. 7. Diurnal course of the hourly mean relative difference in ozone, NO_x and CO concentration [ppb] between the scenario (Albedo, Park) and the base case (Control), with regard to the model mean of 2×2 grid cells for the lowest model level (8.5 m).

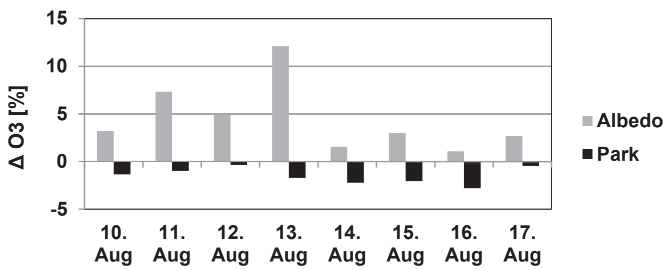

Fig. 8. Relative difference between scenario (Albedo, Park) and base case (Control) for the ozone concentration between 1400 h and 1600 h CEST. Albedo is presented in grey, Park in black.

TKE in the same level. An increase of the turbulent kinetic energy term (TKE) promotes a decrease of CO and NO_x (Fig. 9).

Although the urban greening scenario (Park) shows the highest effect on TKE, the effect on CO and NO_x concentrations is smaller than for the Albedo scenario (Fig 5). The trapping effect of street canyons is still effective when the reflective properties of roofs and wall facades are modified, whereas the Park scenario implies that buildings are completely replaced by natural vegetation. Natural vegetation tends to dissipate sensible heat in favour of latent heat, which in turn decreases the surface temperature and the average height of the boundary layer.

No direct correlation between the concentration of primary pollutants and temperature was found. A change in concentration of one pollutant due to a decrease in atmospheric mixing however can evoke a secondary impact on another compound via chemical reactions. This aspect is discussed in Chapter 5.2.

5.2. Secondary compounds

The lower ozone concentration with temperature reduction cannot be directly explained by a change of atmospheric dynamics as it is valid for the primary pollutants CO and NO_x.

Fig. 10 presents two examples which can be used to explain the decrease of mean ozone concentration simulated for the scenarios Albedo and Park. On the one hand, ozone shows a negative exponential relationship with NO concentration (Fig. 10a). Higher NO due to weaker turbulent mixing leads to a higher rate of NO titration. On the other hand a linear regression can be observed when correlating ozone and temperature (Fig. 10b). No significant correlation was found between simulated primary VOCs (e.g. Formaldehyde HCHO) and ozone concentration.

One of the most important factors which drive photochemical reactions in the troposphere is high energetic shortwave radiation (Seinfeld and Pandis 2012). This aspect explains the increase of peak ozone levels during daytime between 1400 and 1600 CEST when increasing the surface reflectivity (Fig. 7a). Increasing the albedo from 0.2 to 0.7 for the building roofs and facades in the urban canopy model, results in an increase of reflected shortwave radiation. This effect is not observed for the urban greening scenario (Fig 11a). Compared with the urban greening scenario, the Albedo case shows an increase of reflected shortwave radiation by up to 170%. This additional amount of energy accelerates photochemical reactions and by this triggers ozone formation. The increase of ozone for a short period between 1400 and 1600 CEST, leads to the conclusion, that daily averaged ozone concentration can be more efficiently decreased using urban vegetation instead of highly reflective roofs and facades. Fig. 11 b indicates a positive linear relationship between reflected shortwave radiation (SW_UP) [Wm^{-2}] and near surface ozone concentration [ppb]. Fig. 11 c supports this aspect, indicating a positive relationship between the variable SW_UP and the photolysis rate [min^{-1}].

According to Taha (1997a) peak ozone concentrations between 1400 and 1600 h local time for the urban area of Los Angeles and its surroundings decreased by 4.7% when increasing the surface albedo of roofs and walls from 0.2 to 0.5. A similar effect was found for the urban area of Sacramento (Taha, 2008), were the city wide albedo increase reduced peak ozone by about 18%. The maximum temperature reduction in both areas accounted for 4.5 °C and 3 °C respectively. In our study however, an increase in ozone concentration, by up to 12% was found for the Albedo scenario around 1500 CEST. Some possible reasons for this difference may be discussed here making use of the correlations shown in Figs. 10 and 11. Firstly, we apply a higher increase of the albedo of roof and wall surfaces from 0.2 to 0.7 (Takebayashi and Moriyama, 2007) which is 67% more than the increase applied by Taha (1997b, 2008). The resulting reduction in maximum air temperature for the urban area of Stuttgart on the other hand only amounts to 1.5 °C, which is about 1.5–2.5 °C lower than the temperature reduction reported by Taha (1997a; 2008). The reduction of the ozone concentration during most times of the day (Fig. 7) can partly be explained by the temperature decrease which results in reduced ozone formation (Fig. 10). For high solar radiation between 1200 and 1600 CEST, however, the effect of the additional amount of reflected shortwave radiation can partly compensate the temperature effect on chemistry in our Albedo scenario. This is probably not the case in Taha's studies, where the temperature decrease is larger and the increase in reflected solar radiation is less than in our case. Secondly, the larger temperature decrease found by Taha et al. could lead to a more pronounced decrease in turbulent exchange during the day and therefore to a larger increase of the NO_x concentration near the ground. This in turn leads to more ozone titration than in the current study. Finally, emissions and the VOC/NO_x ratio may be different for the considered regions and also the larger extension of the cities in the US as well as different topography can alter the effect of changed urban albedo on ozone concentrations.

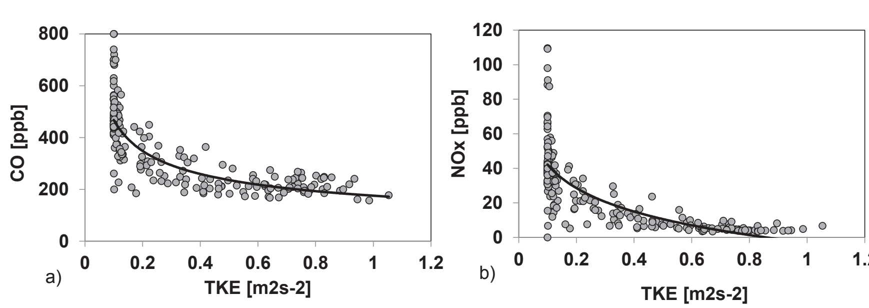

Fig. 9. Dependence of near surface concentration of primary pollutants CO (a) and NOx (b) on turbulent kinetic energy (TKE) for hourly values of the modelling period (Aug 10 – Aug 18 2003). Values are shown for the Control run.

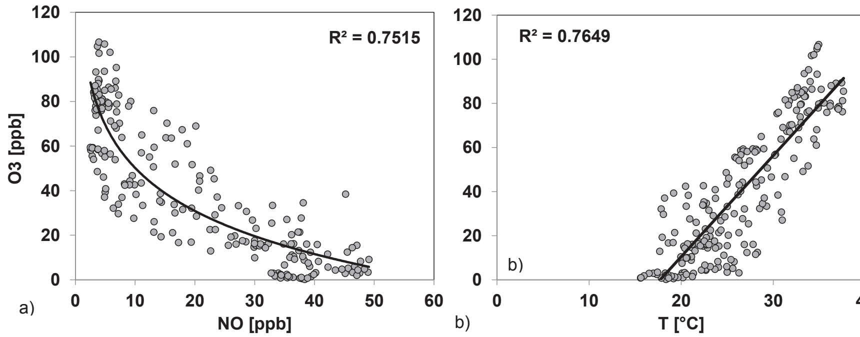

Fig. 10. Correlation between surface NO [ppb] and surface ozone concentration [ppb] (a) and correlation between 2 m potential temperature [°C] and surface ozone concentration [ppb] for hourly model output of the modelling period (Aug 10 – Aug 18 2003) (b). Values are shown for the Control run.

5.3. Analysis of tendency terms

In order to quantify the scenario impact on the concentration of primary and secondary compounds, the respective contributions of physical and chemical processes to the diurnal variation of NO_2, NO, CO and O_3 are analysed on the basis of hourly budgets. These budgets can be retrieved from accumulated tendency terms, provided by WRF-Chem. The base case (Control) and the Albedo scenario are discussed as an example.

The budget terms for the chemical species are the chemical production/loss tendency (CHEM), the turbulent vertical mixing tendency (TURB) and the advective tendency (ADV). The net tendency for a given chemical species can be calculated by adding up these terms, together with the net emission at the grid cell box.

Fig. 12 shows the diurnal variations of the hourly budgets calculated for the lowest model level (~8.5 m) for the city centre. Negative values indicate a loss and positive values a gain for the respective term. In general the turbulence term (TURB) is negative for primary pollutants because turbulent transport results in a dilution of primary compounds which are emitted near the surface.

With a maximum loss of −1000 ppbv h^{-1} at 0800 CEST, turbulent mixing (TURB) is the dominant process for CO (Fig. 12a). The largest negative tendencies are found during the times of the day with maximum emissions during the morning and evening rush hour.

From 0800 am to 1000 CEST, the turbulent kinetic energy is tripled from 0.1 to 0.33 $m^{-2}s^{-2}$ and the PBLH raises from 20 m to 600 m respectively. For the Albedo scenario, both, TKE and PBLH are reduced (Table 5) as compared to the base case. The lower vertical exchange results in a reduced turbulent mixing term (TURB) during the forenoon for the Albedo scenario. Less CO is mixed upward during this time.

The advection term (ADV) for CO shows values ranging from −200 to +300 ppbv h $^{-1}$ for the base case. The positive values during the nighttime can be explained by the contribution of upwind located strong emissions. Due to the complex topography of the Stuttgart area, the wind direction changes in the course of the day from north/north-west during daytime to south/south east during the night. This effect leads to advection of polluted air masses from the industrial areas south-east of Stuttgart into the urban area which results in a positive advection tendency for the grid cells around the urban centre predominately during the evening and night. During the day, ADV is lower and can even turn negative, which indicates an outflow of polluted air from the urban centre as the wind direction has changed to north–north west in the morning again (Supplementary Material Fig. A). For Albedo, the advection term is increased as compared to the base case for most times of the day due to the slightly changed atmospheric dynamics. The chemical term (CHEM) can almost be neglected for CO as it is below 10 ppbv h^{-1}.

For ozone the turbulent term TURB is always positive with maximum values in the morning and in the evening. During this time ozone concentrations are higher in the residual layer than near the surface due to les titration and no loss by deposition and ozone is mixed downward into the surface layer from the residual layer as already described by Zhang and Rao (1999) and by Klein et al. (2014). Simulated ozone profiles supporting this explanation are presented in the Supplementary Material (Fig. B) and were also observed by Velasco et al. (2008). Around noon, when the boundary layer is well mixed and the vertical gradient of the ozone concentration is only small, the turbulent term for ozone shows a local minimum.

In the evening, downward transport from upper layers increases again. Due to the high NO emissions during the morning and evening rush hours, the CHEM term shows local minima at these times as ozone is depleted by NO-titration (Fig. 12b). During nighttime, O_3 at the surface is destroyed by NO as well. Even during daytime the photochemical ozone formation is not able to outperform the titration by NO in the lowest model layer at the regarded location in the city centre. The advection term (ADV) is fluctuating in the range

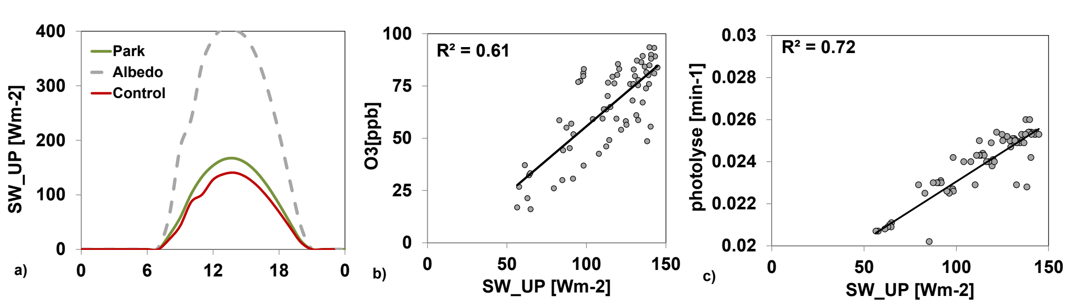

Fig. 11. Mean diurnal course of reflected short-wave radiation (SW_UP) for Control and two scenarios (a). Correlation between reflected shortwave radiation SW_UP and surface concentrations of O_3 (b) and SW_UP and O_3 photolysis rate (c) for hourly model output for the base case (Control).

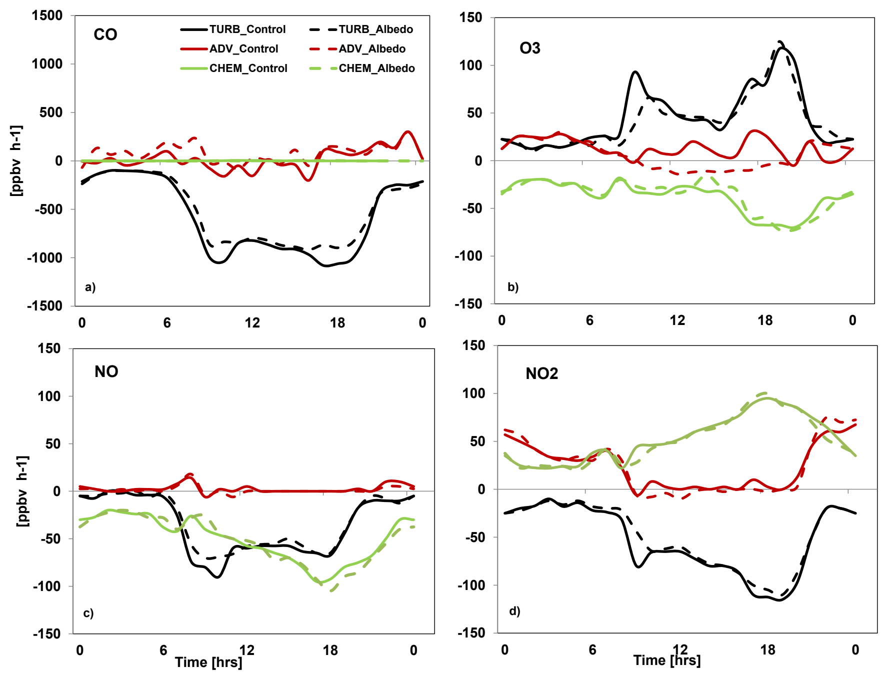

Fig. 12. Diurnal variation of mean hourly budgets of CO (a), O_3 (b) NO (c) and NO_2 (d) with respect to turbulence (TURB), advection (ADV) and chemistry (CHEM) for the Control case and the Albedo scenario for the centre of Stuttgart. The solid line shows the 'Control' case and the dashed line the 'Albedo' scenario.

of $\pm$20 ppb and is positive for the Control Run.

For the Albedo scenario, the turbulent downward flux of ozone is reduced in particular during the morning coming along with a reduction of turbulent mixing. A less negative chemical tendency is observed during most of the daytime with the maximum difference at around 1500 CEST, which can be explained by the higher photolysis due to the strongly enhanced reflected shortwave radiation for the Albedo scenario (Fig 11). This reduction in chemical ozone loss was not found for the 'Park' scenario (see Supplementary Material Fig. C) where the effect of the temperature decrease is dominant and results in enhanced chemical destruction of near surface ozone for all hours of the day. In particular, the less negative peak in the chemical tendency in the afternoon that was found for the Albedo scenario is not present for the CHEM term of the Park scenario. This can explain why maximum ozone concentrations are decreased for the Park scenario and increased for the Albedo scenario (Fig. 8).

For both NO (Fig. 12c) and NO_2 (Fig. 12d), the TURB term is negative during the day, as vertical mixing dilutes the compounds which are emitted near the ground. For NO and NO_2 the TURB term shows negative peaks, corresponding to high levels of emission/concentration. CHEM is reversed for NO and NO_2, as emitted NO is transferred to NO_2 when reacting with ozone. For this term, only a small difference can be found between both scenarios. Same is true for the advection term ADV. ADV can almost be neglected for NO as it quickly reacts to NO_2 and its concentration is close to zero during most times of the day. The high nighttime values of the NO_2 advection term can be explained equivalent to CO. In general, Fig. 12 confirms the impact of a higher albedo on turbulent mixing. The results from this analysis can be compared with the findings of Sarrat et al. (2006) stating the key role of turbulent fluxes on atmospheric chemistry.

6. Conclusion

Simulations with WRF-Chem including the multi-layer urban canopy model BEP were performed for the city of Stuttgart for a summer episode in 2003 in order to point out that well-known urban heat island mitigation measures can also have side effects on urban air quality. This specific period was chosen, because it provides a powerful case study for anticipating the impacts of summertime climate change in Europe (Vautard et al., 2007).

The selected measures can have both positive and negative impacts on primary and secondary pollutants. For the secondary pollutant ozone, our simulation results indicate a decrease in average near surface concentration**s** by 5–8%, when applying urban greening or highly reflective surfaces. The present study could prove that an increase of albedo and urban vegetation is able to improve air quality, leading to reduction of daily mean ozone concentration. By this, it supports findings from previous studies (Taha, 1997a,b, Akbari et al., 2001). With regard to peak ozone concentrations however we simulated an increase by up to 12% for our high albedo scenario whereas Taha (1997a; 2008) report about a decrease in peak ozone. This can be attributed to the stronger albedo increase applied here while the simulated temperature decrease was considerably smaller for Stuttgart than for the US cities in Taha (1997a; 2008).

With regard to the primary pollutants CO or NO_x, the positive effect of reduced temperature is reversed. Model results show, that a temperature reduction has a significant effect on the dynamical structure of the urban boundary layer. A decrease of turbulent kinetic energy (TKE) due to a lower temperature leads to a lower rate of turbulent mixing and a decrease of the mixing layer height, thus resulting in higher near surface concentrations of primary pollutants. This holds in particular for the scenario where the albedo of building roofs and walls was increased resulting in a relative increase in primary pollutants by up to 25% for both, NO_x and CO.

It was not the purpose of this paper however to develop a recommendation for the implementation of a specific measure, as different positive and negative effects have to be traded off against each other and more detailed studies will be required for such a decision. Our paper provides a modelling case study for a Mid-European city. For cities with different size, location, population density, emission or meteorological conditions the same measures might have different effects on air quality.

The effects explained before do also not consider a change in emissions, which practically would be the most efficient strategy to improve urban air quality. Furthermore, this case study deals only with meteorological conditions found for a clear sky, sunny period in summer.

Within applied urban planning, the social effect of a park, increasing the well-being of the urban dwellers, has to be taken into account as well. However, the tree species planted in the park must be carefully chosen in order to avoid an increase in ozone concentrations due to increased biogenic VOC emissions (Donovan et al., 2005). The role of biogenic emissions and their function as precursor substances to a number of chemical reactions is in the focus of current and previous scientific work in the field of urban air quality (Chameides et al., 1988; Grote et al., 2013). Rising temperature under future climate conditions can increase the emission of BVOCs, thus increasing ozone concentration for instance. Finding strategies to avoid that urban greening can also negatively affect the air quality by the emission of biogenic compounds is considered to be a major challenge in future studies.

Acknowledgement

This work is funded by the EU- Project “UHI - Development and application of mitigation and adaptation strategies and measures for counteracting the global UHI phenomenon” (3CE292P3) – CENTRAL Europe. (2011–2014). The authors also thanks the Office for Environmental Protection; Department for Urban Climate from the Capital City of Stuttgart, the Institute of Environmental Protection of the federal state of Baden-Württemberg, the University of Hohenheim and land surveying office Stuttgart for collaboration and observation data. Further acknowledgement goes to Hugo Denier van der Gon (TNO) for providing the emission inventory and NOAA, Boulder for the access to the computing environment there in the course of an internship within the working group of Dr. Georg Grell. This internship was made possible with funding from the KIT Graduate School on Climate and Environment (GRACE).

Appendix A. Supplementary data

Supplementary data related to this article can be found at http://dx.doi.org/10.1016/j.atmosenv.2015.10.094.

References

Ackermann, I.J., Hass, H., Memmesheimer, M., Ebel, A., Binkowski, F.S., Shankar, U., 1998. Modal aerosol dynamics model for Europe: development and first applications. Atmos. Environ. 32 (17), 2981–2999.

Akbari, H., Pomerantz, M., Taha, H., 2001. Cool surfaces and shade trees to reduce energy use and improve air quality in urban areas. Sol. Energy 70 (3), 295–310.

Akbari, H., Bretz, S., Kurn, D.M., Hanford, J., 1997. Peak power and cooling energy savings of high-albedo roofs. Energy Build. 25 (2), 117–126.

Akbari, H., Menon, S., Rosenfeld, A., 2009. Global cooling: increasing world-wide urban albedos to offset CO2. Clim. Change 94 (3–4), 275–286. http://dx.doi.org/10.1007/s10584-008-9515-9. Available from:

Arnfield, A.J., 2003. Two decades of urban climate research: a review of turbulence, exchanges of energy and water, and the urban heat island. Int. J. Climatol. 23 (1), 1–26. http://dx.doi.org/10.1002/joc.859. Available from:

Barlow, J.F., Halios, C.H., Lane, S.E., Wood, C.R., 2015. Observations of urban boundary layer structure during a strong urban heat island event. Environ. Fluid Mech. 15 (2), 373–398. http://dx.doi.org/10.1007/s10652-014-9335-6. Available from:

Chameides, W.L., Lindsay, R.W., Richardson, J., Kiang, C.S., 1988. The role of biogenic hydrocarbons in urban photochemical smog: Atlanta as a case study. Science 241 (4872), 1473–1475. Available from: http://www.sciencemag.org/content/241/4872/1473.abstract.

Chen, F., Kusaka, H., Bornstein, R., Ching, J., Grimmond, C.S.B., Grossman-Clarke, S., Loridan, T., Manning, K.W., Martilli, A., Miao, S., Sailor, D., Salamanca, F.P., Taha, H., Tewari, M., Wang, X., Wyszogrodzki, A.A., Zhang, C., 2011. The integrated WRF/urban modeling system: development, evaluation, and applications to urban environmental problems. Int. J. Climatol. 31 (2), 273–288. http://dx.doi.org/10.1002/joc.2158. Available from:

Dee, D.P., Uppala, S.M., Simmons, A.J., Berrisford, P., Poli, P., Kobayashi, S., Andrae, U., Balmaseda, M.A., Balsamo, G., Bauer, P., Bechtold, P., Beljaars, A.C.M., van de Berg, L., Bidlot, J., Bormann, N., Delsol, C., Dragani, R., Fuentes, M., Geer, A.J., Haimberger, L., Healy, S.B., Hersbach, H., H+¦lm, E.V., Isaksen, L., K+Ñllberg, P., K+Âhler, M., Matricardi, M., McNally, A.P., Monge-Sanz, B.M., Morcrette, J.J., Park, B.K., Peubey, C., de Rosnay, P., Tavolato, C., Thepaut, J.N., Vitart, F., 2011. The ERA-Interim reanalysis: configuration and performance of the data assimilation system. Q. J. R. Meteorol. Soc. 137 (656), 553–597. http://dx.doi.org/10.1002/qj.828. Available from:

De Ridder, K., Lauwaet, D., Maiheu, B., 2015. UrbClim GÇô A fast urban boundary layer climate model. Urban Clim. 12 (0), 21–48. Available from: http://www.sciencedirect.com/science/article/pii/S2212095515000024.

Donovan, R.G., Stewart, H.E., Owen, S.M., MacKenzie, A.R., Hewitt, C.N., 2005. Development and application of an urban tree air quality score for photochemical pollution episodes using the Birmingham, United Kingdom, area as a case study. Environ. Sci. Technol. 39 (17), 6730–6738.

Emmons, L.K., Walters, S., Hess, P.G., Lamarque, J.F., Pfister, G.G., Fillmore, D., Granier, C., Guenther, A., Kinnison, D., Laepple, T., Orlando, J., Tie, X., Tyndall, G., Wiedinmyer, C., Baughcum, S.L., Kloster, S., 2010. Description and evaluation of the model for ozone and related chemical Tracers, version 4 (MOZART-4). Geosci. Model Dev. 3 (1), 43–67. Available from: http://www.geosci-model-dev.net. /3/43/2010/.

Fallmann, J., Emeis, S., Suppan, P., 2014. Mitigation of urban heat stress - a modeling case study for the area of Stuttgart. DIE ERDE J. Geogr. Soc. Berl. 144 (3–4), 202–216.

Georgescu, M., Morefield, P.E., Bierwagen, B.G., Weaver, C.P., 2014. Urban adaptation can roll back warming of emerging megapolitan regions. Proc. Natl. Acad. Sci. 111 (8), 2909–2914. Available from: http://www.pnas.org/content/111/8/2909.abstract.

Giannaros, T.M., Melas, D., Daglis, I.A., Keramitsoglou, I., Kourtidis, K., 2013. Numerical study of the urban heat island over Athens (Greece) with the WRF model. Atmos. Environ. 73 (0), 103–111. Available from: http://www.sciencedirect.com/science/article/pii/S1352231013001726.

Giordano, L., Brunner, D., Flemming, J., Hogrefe, C., Im, U., Bianconi, R., Badia, A., Balzarini, A., Bar¦, R., Chemel, C., Curci, G., Forkel, R., Jimenez-Guerrero, P., Hirtl, M., Hodzic, A., Honzak, L., Jorba, O., Knote, C., Kuenen, J.J.P., Makar, P.A., Manders-Groot, A., Neal, L., Perez, J.L., Pirovano, G., Pouliot, G., San Jose, R., Savage, N., Schräder, W., Sokhi, R.S., Syrakov, D., Torian, A., Tuccella, P., Werhahn, J., Wolke, R., Yahya, K., Zabkar, R., Zhang, Y., Galmarini, S., 2015. Assessment of the MACC reanalysis and its influence as chemical boundary conditions for regional air quality modeling in AQMEII-2. Atmos. Environ. 115 (0), 371–388. http://www.sciencedirect.com/science/article/pii/S1352231015001533.

Grell, G.A., Devenyi, D., 2002. A generalized approach to parameterizing convection combining ensemble and data assimilation techniques. Geophys. Res. Lett. 29 (14) http://dx.doi.org/10.1029/2002GL015311.

Grell, G.A., Peckham, S.E., Schmitz, R., McKeen, S.A., Frost, G., Skamarock, W.C., Eder, B., 2005. Fully coupled “online” chemistry within the WRF model. Atmos. Environ. 39 (37), 6957–6975.

Grote, R., Monson, R., Niinemets, 2013. Leaf-level models of constitutive and stress-driven volatile organic compound emissions. In: Niinemets, Monson, R.K. (Eds.), Biology, Controls and Models of Tree Volatile Organic Compound Emissions, fifth ed. Springer, Netherlands, pp. 315–355. +. l.

Guenther, A.B., Jiang, X., Heald, C.L., Sakulyanontvittaya, T., Duhl, T., Emmons, L.K., Wang, X., 2012. The model of emissions of gases and aerosols from nature version 2.1 (MEGAN2.1): an extended and updated framework for modeling biogenic emissions. Geosci. Model Dev. 5 (6), 1471–1492. Available from: http://www.geosci-model-dev.net/5/1471/2012/.

Hu, X.M., Nielsen-Gammon, J.W., Zhang, F., 2010. Evaluation of three planetary boundary layer schemes in the WRF model. J. Appl. Meteorol. Climatol. 49 (9), 1831–1844.

Im, U., Bianconi, R., Solazzo, E., Kioutsioukis, I., Badia, A., Balzarini, A., Baro, R., Bellasio, R., Brunner, D., Chemel, C., Curci, G., Flemming, J., Forkel, R., Giordano, L., Jimenez-Guerrero, P., Hirtl, M., Hodzic, A., Honzak, L., Jorba, O., Knote, C., Kuenen, J.J.P., Makar, P.A., Manders-Groot, A., Neal, L., Perez, J.L., Pirovano, G., Pouliot, G., San Jose, R., Savage, N., Schröder, W., Sokhi, R.S., Syrakov, D., Torian, A., Tuccella, P., Werhahn, K., Wolke, R., Yahya, K., Žabkar, R., Zhang, Y., Zhang, J., Hogrefe, C., Galmarini, S., 2015. Evaluation of operational online-coupled regional air quality models over Europe and North America in the context of AQMEII phase2. Part I: ozone. Atmos. Environ. 115, 404–420. http://dx.doi.org/10.1016/j.atmosenv.2014.09.042.

Janjiç, Z.I., 1990. The step-mountain coordinate: physical package. Mon. Weather Rev. 118 (7), 1429–1443. http://dx.doi.org/10.1175/1520-0493(1990)118<1429:TSMCPP>2.0.CO;2. Available from:(accessed 30.12.14.).

Janjic, 2001. Nonsingular implementation of the Mellor-Yamadalevel 2.5 scheme in the NCEP meso model. NOAA/NWS/NCEP Off. Note 437, 61.

Klein, P., Hu, X.M., Xue, M., 2014. Impacts of mixing processes in nocturnal atmospheric boundary layer on urban ozone concentrations. Bound. Layer Meteorol. 150 (1), 107–130. http://dx.doi.org/10.1007/s10546-013-9864-4. Available from:

Knote, Ch, Tuccella, P., Curci, G., Emmons, L., Orlando, J.J., Madronich, S., Baró, R., Jiménez-Guerrero, P., Luecken, D., Hogrefe, C., Forkel, R., Werhahn, J., Hirtl, M., Pérez, J.L., San José, R., Giordano, L., Brunner, D., Khairunnisa, Y., Zhang, Y., 2015. Influence of the choice of gas-phase mechanism on predictions of key gaseous pollutants during the AQMEII phase-2 intercomparison. Atmos. Environ. 115,

553–568. http://dx.doi.org/10.1016/j.atmosenv.2014.11.066.
Kuenen, J., van der Gon, H.D., Visschedijk, A., van der Brugh, H., van Gijlswijk, R., 2011. MACC European Emission Inventory for the Years 2003–2007. TNO-report TNO-060-UT-2011–00588, Utrecht.
Kusaka, H., Kondo, H., Kikegawa, Y., Kimura, F., 2001. A simple single-layer urban canopy model for atmospheric models: comparison with multi-layer and slab models. Bound. Layer Meteorol. 101 (3), 329–358. http://dx.doi.org/10.1023/A%3A1019207923078. Available from:
Lai, L.W., Cheng, W.L., 2009. Air quality influenced by urban heat island coupled with synoptic weather patterns. Sci. Total Environ. 407 (8), 2724–2733. Available from: http://www.sciencedirect.com/science/article/pii/S0048969708012576.
Lin, Y.-L., Farley, R.D., Orville, H.D., 1983. Bulk parameterization of the snow field in a cloud model. J. Clim. Appl. Meteorol. 22, 1065–1092.
Mellor, G.L., Yamada, T., 1982. Development of a turbulence closure model for geophysical fluid problems. Rev. Geophys. 20 (4), 851–875. http://dx.doi.org/10.1029/RG020i004p00851. Available from:
Martilli, A., Clappier, A., Rotach, M., 2002. An urban surface exchange parameterisation for mesoscale models. Bound. Layer Meteorol. 104 (2), 261–304. http://dx.doi.org/10.1023/A%3A1016099921195. Available from:
Mitchell, K.N.&C., 2005. The Community Noah Land-surface Model (LSM) – User's Guide. Public Release Version 2.7.1.2005. http:/www.ral.ucar.edu/research/land/technology/lsm/noah/Noah_LSM_USERGUIDE_2.7.1.pdf.
Mlawer, E.J., Taubman, S.J., Brown, P.D., Iacono, M.J., Clough, S.A., 1997. Radiative transfer for inhomogeneous atmospheres: RRTM, a validated correlated-k model for the longwave. J. Geophys. Res. Atmos. 102 (D14), 16663–16682. http://dx.doi.org/10.1029/97JD00237. Available from:
Oke, T.R., 1982. The energetic basis of the urban heat island. Q. J. R. Meteorol. Soc. 108 (455), 1–24. http://dx.doi.org/10.1002/qj.49710845502. Available from:
Salamanca, F., Martilli, A., 2012. A numerical study of the urban heat island over Madrid during the DESIREX (2008) campaign with WRF and an evaluation of simple mitigation strategies. Int. J. Climatol. 32 (15), 2372–2386. http://dx.doi.org/10.1002/joc.3398. Available from:
Santamouris, M., 2007. Heat island research in Europe: the state of the art. Adv. Build. Energy Res. 1 (1), 123–150. Available from: http://dx.doi.org/10.1080/17512549.2007.9687272 (accessed 07.07.15.).
Sarrat, C., Lemonsu, A., Masson, V., Guedalia, D., 2006. Impact of urban heat island on regional atmospheric pollution. Atmos. Environ. 40 (10), 1743–1758. Available from: http://www.sciencedirect.com/science/article/pii/S1352231005010885.
Schell, B., Ackermann, I.J., Hass, H., Binkowski, F.S., Ebel, A., 2001. Modeling the formation of secondary organic aerosol within a comprehensive air quality model system. J. Geophys. Res. 106, 28.
Schubert, S., Grossman-Clarke, S., 1–4-2013. The influence of green areas and roof albedos on air temperatures during extreme heat events in Berlin, Germany. Meteorol. Z. 22 (2), 131–143.
Seinfeld, J.H., Pandis, S.N., 2012. Atmospheric Chemistry and Physics: from Air Pollution to Climate Change. John Wiley & Sons.
Stull, R.B., 1988. An Introduction to Boundary Layer Meteorology, 13 ed. Springer.
Taha, H., 1997a. Modeling the impacts of large-scale albedo changes on ozone air quality in the South Coast air Basin. Atmos. Environ. 31 (11), 1667–1676. Available from: http://www.sciencedirect.com/science/article/pii/S1352231096003366.
Taha, H., 1997b. Urban climates and heat islands: albedo, evapotranspiration, and anthropogenic heat. Energy Build. 25 (2), 99–103. Available from: http://www.sciencedirect.com/science/article/pii/S0378778896009991.
Taha, H., 2008. Meso-urban meteorological and photochemical modeling of heat island mitigation. Atmos. Environ. 42 (38), 8795–8809. Available from: http://www.sciencedirect.com/science/article/pii/S1352231008006158.
Takebayashi, H., Moriyama, M., 2007. Surface heat budget on green roof and high reflection roof for mitigation of urban heat island. Build. Environ. 42 (8), 2971–2979. Available from: http://www.sciencedirect.com/science/article/pii/S0360132306001752.
Tam, B.Y., Gough, W.A., Mohsin, T., 2015. The impact of urbanization and the urban heat island effect on day to day temperature variation. Urban Clim. 12 (0), 1–10. Available from: http://www.sciencedirect.com/science/article/pii/S2212095514001126.
USGS, 2006. The National Land Cover Database. Accessed at. http://landcover.usgs.gov/usgslandcover.php, 05/25/2014.
Vautard, R., Beekmann, M., Desplat, J., Hodzic, A., Morel, S., 2007. Air quality in Europe during the summer of 2003 as a prototype of air quality in a warmer climate. Comptes Rendus Geosci. 339 (11–12), 747–763.
Velasco, E., Marquez, C., Bueno, E., Bernabe, R.M., Sanchez, A., Fentanes, O., Wöhrnschimmel, H., Cardenas, B., Kamilla, A., Wakamatsu, S., Molina, L.T., 2008. Vertical distribution of ozone and VOCs in the low boundary layer of Mexico City. Atmos. Chem. Phys. 8 (12), 3061–3079. Available from: http://www.atmos-chem-phys.net/8/3061/2008/.
Wang, Wei, Barker, Dale, Bray, John, Bruyere, Cindy, Duda, Michael, Dudhia, Jimy, Gill, Dave, Michalakes, John, 2011. User's Guide for Advanced Research WRF (ARW) Modeling System Version 3.
Wesely, M.L., 1989. Parameterization of surface resistances to gaseous dry deposition in regional-scale numerical models. Atmos. Environ. (1967) 23 (6), 1293–1304.
Wesely, M.L., Hicks, B.B., 2000. A review of the current status of knowledge on dry deposition. Atmos. Environ. 34 (12GÇô14), 2261–2282. Available from: http://www.sciencedirect.com/science/article/pii/S1352231099004677.
Wood, C.R., Järvi, L., Kouznetsov, R.D., Nordbo, A., Joffre, S., Drebs, A., Vihma, T., Hirsikko, A., Suomi, I., Fortelius, C., O'Connor, E., Moiseev, D., Haapanala, S., Moilanen, J., Kangas, M., Karppinen, A., Vesala, T., Kukkonen, J., 2013. An overview of the urban boundary layer atmosphere network in Helsinki. Bull. Am. Meteorol. Soc. 94 (11), 1675–1690. http://dx.doi.org/10.1175/BAMS-D-12-00146.1. Available from:(accessed 13.08.15.).
Zaksek, K., Ostir, K., 2012. Downscaling land surface temperature for urban heat island diurnal cycle analysis. Remote Sens. Environ. 117 (0), 114–124. Available from: http://www.sciencedirect.com/science/article/pii/S0034425711002872.
Zhang, J., Rao, S.T., 1999. The role of vertical mixing in the temporal evolution of ground-level ozone concentrations. J. Appl. Met. 38, 1674–1691.
Zhou, J., Chen, Y., Zhang, X., Zhan, W., 2013. Modeling the diurnal variations of urban heat islands with multi-source satellite data. Int. J. Remote Sens. 34 (21), 7568–7588. http://dx.doi.org/10.1080/01431161.2013.821576. Available from: (accessed 07.07.15.).